Spectral Domain Iterative Analysis of Single- and Double-Layered Microstrip Antennas Using the Conjugate Gradient Algorithm

RAPHAEL KASTNER, SENIOR MEMBER, IEEE, EHUD HEYMAN, SENIOR MEMBER, IEEE, AND ALBERT SABBAN

Abstract—**An analysis for single- and double-layered microstrip antennas is described. The planarity of these structures makes it possible to construct a general spectral representation for any number of layers and to derive the spectral Green's dyad in a compact fashion using a transmission line analogy. A formulation of the antenna problem in the spectral domain, incorporating this dyad, is coupled with the conjugate gradient (CG) algorithm, whose applicability as an efficient way of analyzing a number of microstrip antennas is studied. Results appear to be quite accurate. Conclusions pertaining to the applicability of the method, including effects of problem parameters on convergence rates, are drawn.**

I. Introduction

TO DATE, a number of computational approaches for microstrip antennas analysis have been developed for certain configurations and a range of accuracies. Some of these methods are restricted to geometries such as rectangular or circular patches only. Others are restricted in terms of structure size or attainable accuracy. Virtually all of them are applicable to single-layered antennas. Perhaps the simplest way to analyze a rectangular single patch antenna is the double slot, or transmission line model [2]–[7]. It can provide reasonable radiation pattern prediction; however, it is not extendable to more complicated geometries. The cavity model [8]–[11] makes it possible to convert the open antenna problem into a closed one, thereby achieving a good prediction of impedances and radiation characteristics of thin single-layered separable structures. More general approaches, based on the moment method, include a representation of the antenna by a wire grid model [12], or the decomposition of the current distribution into entire domain basis functions [13]–[15], and possess the well-known advantages and disadvantages of the moment method. Additional specific approaches are also available [16], [17]. As for double- or multiple-layered structures, we are aware of an approach for narrow double-layered dipoles [18]. However, the wide-band stacked double-layered antenna, introduced recently by Sabban [1] and quoted by Chen [19], has not received attention in that regard yet.

In this work, the conjugate gradient (CG) algorithm is studied as a potentially efficient way for accurately computing radiation patterns of general microstrip antennas. It is formulated along the lines suggested by Van Den Berg [20], which are based on the original scheme introduced in [21] and quoted widely (e.g., [22]). The algorithm is combined with a spectral domain formulation of the problem [23], utilizing a spectral Green's dyad for the grounded multilayered dielectric slab. The construction of this dyad for any number of layers begins our discussion in Section II. A systematic process based on a proper scalarization of the spectral field equations [24] provides a general spectral modeling of layered structures and greatly simplifies the derivation of the Green's dyad. With the dyad at hand, the problem may be formulated in the spectral domain as discussed in Section III. Next, the CG algorithm is tailored to the single- and double-layered cases in Section IV. Results for both cases are subsequently described in Section V, and the convergence properties of the algorithm are presented. In particular, geometry is shown to be one dominant factor affecting convergence rate. Prediction of measured radiation patterns is very good, including the cross-polarized component. The method is thus established as an alternative tool for the analysis of general microstrip structures though not without its limitations, as outlined in the conclusions (Section VI).

Manuscript received December 12, 1986; revised July 3, 1987.

R. Kastner and A. Sabban are with RAFAEL, P.O. Box 2250/87, Haifa 31021, Israel.

E. Heyman is with the Department of Electrical Engineering, Tel Aviv University, Tel Aviv 69978, Israel.

IEEE Log Number 8821976.

II. Spectral Domain Green's Dyad for Layered Structures

The grounded multilayered dielectric slab, shown in Fig. 1, forms the model for the Green's dyad derivation. It can have continuous as well as discontinuous variations in the z direction. Being uniform throughout the x–y plane, though, it lends itself to transmission line analogy [24] where the scalar potential functions ϕ and ψ for the transverse electric (TE) and transverse magnetic (TM) spectral modes, respectively, are just Fourier kernels:

$$\phi(x, y; k_x, k_y) = \psi(x, y; k_x, k_y) = \frac{1}{2\pi} e^{-j(k_x x + k_y y)}. \quad (1)$$

The actual field is synthesized now by a superposition of all the spectral modes which, in view of (1), reads (we use the electric field as an example)

$$\mathbf{E}(x, y, z) = \int\int \tilde{\mathbf{E}}(k_x, k_y, z)\phi(x, y; k_x, k_y)\, dk_x\, dk_y = F^{-1}\{\tilde{\mathbf{E}}(k_x, k_y, z)\} \quad (2)$$

where the tilde denotes a spectral field quantity. These

0018-926X/88/0900-1204$01.00

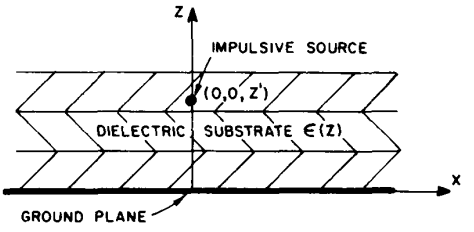

Fig. 1. Multilayered grounded structure excited by point source.

potentials, containing the spatial dependence on x and y, are suppressed in the sequel, leaving the spectral representation $\tilde{\mathbf{E}}$ as the remainder. Once this is done, a transmission line equivalent for each spectral mode may be formulated using modal voltages and currents, $\tilde{V}$ and $\tilde{I}$, respectively, that define the spectral transverse electric and magnetic fields via

$$\tilde{\mathbf{E}}_t'(\mathbf{k}_t, z) = j\hat{\mathbf{p}}\tilde{V}'(\mathbf{k}_t, z) \qquad \tilde{\mathbf{E}}_t''(\mathbf{k}_t, z) = -j\hat{\mathbf{q}}\tilde{V}''(\mathbf{k}_t, z) \tag{3a}$$

$$\tilde{\mathbf{H}}_t'(\mathbf{k}_t, z) = j\hat{\mathbf{q}}\tilde{I}'(\mathbf{k}_t, z) \qquad \tilde{\mathbf{H}}_t''(\mathbf{k}_t, z) = j\hat{\mathbf{p}}\tilde{I}''(\mathbf{k}_t, z). \tag{3b}$$

Here the single and double prime notations denote the TM and TE modes, respectively, and we use the vector notation

$$\mathbf{k}_t = k_x\hat{\mathbf{x}} + k_y\hat{\mathbf{y}} \qquad k_t = \sqrt{k_x^2 + k_y^2}$$
$$\hat{\mathbf{p}} = \mathbf{k}_t/k_t \qquad \hat{\mathbf{q}} = \hat{\mathbf{z}} \times \hat{\mathbf{p}} \tag{4}$$

with the carets denoting unit vectors. The corresponding longitudinal field components are

$$\tilde{E}_z'(\mathbf{k}_t, z) = \frac{1}{j\omega\epsilon(z)}\left[k_t\tilde{I}'(\mathbf{k}_t, z) - \tilde{J}_z(\mathbf{k}_t, z)\right] \tag{5a}$$

$$\tilde{H}_z''(\mathbf{k}_t, z) = \frac{1}{j\omega\mu_0}k_t\tilde{V}''(\mathbf{k}_t, z) \tag{5b}$$

where $\tilde{\mathbf{J}}_z$ is the longitudinal component of the spectral current. The spectral amplitude functions now satisfy the transmission line equation

$$-\frac{d\tilde{V}}{dz} = jk_z\tilde{Z}\tilde{I} + \tilde{v} \qquad -\frac{d\tilde{I}}{dz} = jk_z\tilde{Y}\tilde{V} + \tilde{i}. \tag{6}$$

Here, the characteristic impedances for the TM and TE modes are given, respectively, by

$$\tilde{Z}' = \frac{1}{\tilde{Y}'} = Z(z)\frac{k_z(z)}{k(z)} \qquad \tilde{Y}'' = \frac{1}{\tilde{Z}''} = Y(z)\frac{k_z(z)}{k(z)} \tag{7}$$

where $Z(z) = Y^{-1}(z) = \sqrt{\mu_0/\epsilon(z)}$, $k(z) = \omega\sqrt{\mu_0\epsilon(z)}$, and

$$k_z(z) = \sqrt{k^2(z) - k_t^2}. \tag{8}$$

In (6), $\tilde{v}$ and $\tilde{i}$ denote the transmission line equivalent voltage or current sources, respectively, obtained from the spectral currents via

$$\tilde{v}' = j\frac{k_t}{\omega\epsilon(z)}\tilde{J}_z \qquad \tilde{i}'(\mathbf{k}_t, z) = -j\hat{\mathbf{p}}\cdot\tilde{\mathbf{J}}$$
$$\tilde{i}''(\mathbf{k}_t, z) = j\hat{\mathbf{q}}\cdot\tilde{\mathbf{J}} \qquad \tilde{v}''(\mathbf{k}_t, z) = 0. \tag{9}$$

To obtain an expression for the spectral dyadic Green's function, we consider impulsive sources located at the $z = z'$ plane, so that

$$\tilde{v}(z) = \tilde{v}_0\delta(z - z') \qquad \tilde{i}(z) = \tilde{i}_0\delta(z - z'). \tag{10}$$

We now denote the transmission line solutions for unit voltage or current sources in (10) (i.e., $\tilde{v}_0 = 1$, $\tilde{i}_0 = 0$ or $\tilde{i}_0 = 1$, $\tilde{v}_0 = 0$) as $\tilde{V}_v(z, z')$, $\tilde{I}_v(z, z')$ and $\tilde{V}_i(z, z')$, $\tilde{I}_i(z, z')$, respectively. Once the relationships (3), (5), and (9) for the actual fields and currents are combined with the transmission line analog in (6) and (10), one obtains the dyadic Green's relationship

$$\tilde{\mathbf{E}}(z) = \underline{\tilde{\mathbf{G}}}^e(z, z')\cdot\tilde{\mathbf{J}}(z'), \quad \tilde{\mathbf{H}}(z) = \underline{\tilde{\mathbf{G}}}^h(z, z')\cdot\tilde{\mathbf{J}}(z') \tag{11}$$

where the electric dyad is given by

$$\begin{aligned}\underline{\tilde{\mathbf{G}}}^e(z, z') &= \hat{\mathbf{p}}\hat{\mathbf{p}}\tilde{V}_i'(z, z') + \hat{\mathbf{q}}\hat{\mathbf{q}}\tilde{V}_i''(z, z') \\ &\quad - \hat{\mathbf{p}}\hat{\mathbf{z}}\frac{k_t}{\omega\epsilon(z')}\tilde{V}_v'(z, z') - \hat{\mathbf{z}}\hat{\mathbf{p}}\frac{k_t}{\omega\epsilon(z)}\tilde{I}_i'(z, z') \\ &\quad + \hat{\mathbf{z}}\hat{\mathbf{z}}\left[\frac{k_t^2}{\omega^2\epsilon(z)\epsilon(z')}\tilde{I}_v'(z, z') - \frac{1}{j\omega\epsilon(z)}\delta(z - z')\right].\end{aligned} \tag{12}$$

Similar expressions may be obtained for the magnetic dyad, but it will not be used in the sequel. It should be pointed out that, since the functions $\tilde{V}_v$, $\tilde{I}_v$, $\tilde{V}_i$, and $\tilde{I}_i$ are related via the transmission line equation and reciprocity, it is sufficient to solve this equation *only* for the *fundamental solutions* $\tilde{I}_v'$ and $\tilde{V}_i''$ for TM and TE, respectively, and then determine the other solutions via

$$\tilde{I}_i'(z, z') = -\tilde{V}_v'(z', z) = (jk_z\tilde{Y}')^{-1}\frac{d}{dz'}\tilde{I}_v'(z, z') \tag{13a}$$

$$\tilde{V}_v''(z, z') = -\tilde{I}_i''(z', z) = (jk_z\tilde{Z}')^{-1}\frac{d}{dz'}\tilde{V}_i''(z, z'). \tag{13b}$$

III. Spectral Formulation of the Multilayered Antenna Problem

When applying the aforementioned spectral representation to the analysis of antennas comprising N layers, one is interested only in the transverse currents $\tilde{\mathbf{J}}_n$ and transverse electric field $\tilde{\mathbf{E}}_n$ at the nth plane $z = z_n$ of the nth patch. These field components are related via the dyadic Green's function, but they should also satisfy the boundary condition at the nth layer. Denoting by D_n the conducting area (patch) at the z_n plane and defining θ_n as a truncation operator to D_n and $\bar{\theta}_n$ as its complement, one has the following set of $2N$ equations for

the unknowns $\tilde{\mathbf{E}}_n$ and $\tilde{\mathbf{J}}_n$ in the general N layered structure:

$$\theta_n F^{-1}\left[\tilde{\mathbf{E}}_n^{\text{inc}}+\sum_{j=1}^{N}\underline{\tilde{\mathbf{G}}}_{n,j}^{e}\cdot\tilde{\mathbf{J}}_j\right]=0,\qquad n=1,\cdots,N \tag{14a}$$

$$\bar{\theta}_n\tilde{\mathbf{J}}_n=0,\qquad n=1,\cdots,N \tag{14b}$$

where $\tilde{\mathbf{E}}_n^{\text{inc}}$ denotes the incident field at the nth plane (see (19) below) and $\underline{\tilde{\mathbf{G}}}_{n,j}^{e}$, $j=1,\cdots,N$, are the two-by-two electric current dyads that express the contribution of the transverse current $\tilde{\mathbf{J}}_j$ to the transverse field $\tilde{E}_n$ via

$$\tilde{\mathbf{E}}_n=\underline{\tilde{\mathbf{G}}}_{n,j}^{e}\cdot\tilde{\mathbf{J}}_j,\qquad j=1,2,\cdots,N. \tag{15}$$

In view of (12), these dyads are given by

$$\underline{\tilde{\mathbf{G}}}_{n,j}^{e}=\hat{\mathbf{p}}\hat{\mathbf{p}}\,\tilde{V}_i'(z_n,z_j)+\hat{\mathbf{q}}\hat{\mathbf{q}}\,V_i''(z_n,z_j), \tag{16}$$

and their Cartesian form is obtained by using

$$\hat{\mathbf{p}}\hat{\mathbf{p}}=\frac{1}{k_t^2}\begin{bmatrix}k_x^2 & k_xk_y\\ k_xk_y & k_y^2\end{bmatrix}\qquad \hat{\mathbf{q}}\hat{\mathbf{q}}=\frac{1}{k_t^2}\begin{bmatrix}k_y^2 & -k_xk_y\\ -k_xk_y & k_x^2\end{bmatrix} \tag{17}$$

where we have used a matrix notation for the Cartesian dyads. Special attention has to be given to the spectral point $k_x = k_y = 0$ since, from (17), it looks as if the dyad $\underline{\tilde{\mathbf{G}}}_{n,j}^{e}$ has a pole there ($k_t^2 = 0$). However, recalling that $k_t = 0$ defines a TEM mode, one has $\tilde{V}_i' = \tilde{V}_i'' = \tilde{V}_i^0$ where $\tilde{V}_i^0$ denotes a TEM solution, and noting that $\hat{\mathbf{p}}\hat{\mathbf{p}} + \hat{\mathbf{q}}\hat{\mathbf{q}} = \hat{\mathbf{x}}\hat{\mathbf{x}} + \hat{\mathbf{y}}\hat{\mathbf{y}}$, (16) for $k_t = 0$ takes the regular form

$$\underline{\tilde{\mathbf{G}}}_{n,j}^{e}\big|_{k_t=0}=(\hat{\mathbf{x}}\hat{\mathbf{x}}+\hat{\mathbf{y}}\hat{\mathbf{y}})\,\tilde{V}_i^0(z_n,z_j). \tag{18}$$

The antenna problem is solved now by transforming it into the scattering formulation. This is done by defining the incident field as being generated by the feeding structure in the absence of the metallic patches. An idealized, z-directed elementary probe located at $z = z_1$ is being visualized as generating this incident field. This idealization provides a convenient way of computing patterns and perhaps radiation resistance; however, calculation of antenna reactance should require more precise feed modeling. The transverse incident electric field $\tilde{\mathbf{E}}_t^{\text{inc}}$ at any patch plane is then computed from this source and from the Green's vector terms $\tilde{\mathbf{G}}_{tz}^{e}$ relating longitudinal current and transverse electric fields (cf. (12)):

$$\tilde{\mathbf{E}}_t^{\text{inc}}(\mathbf{k}_t,z)=\tilde{\mathbf{G}}_{tz}^{e}(z,z')\tilde{J}_z(z')$$

$$\tilde{\mathbf{G}}_{tz}^{e}(z,z')=-\hat{\mathbf{p}}\,\frac{k_t}{\omega\epsilon(z')}\,\tilde{V}_v'(z,z'). \tag{19}$$

Since the function $\tilde{V}_v'$ is discontinuous in the source region (cf. (13a)), we shall assume that the probe is located slightly below the patch at $z' = z_1^-$. The specific form of the Green's dyads depends now on the transmission line solutions $\tilde{V}_i'$ and $\tilde{V}_i''$. As an example, we shall write these expressions explicitly for the single- and double-layered antennas, for which numerical calculations have been done.

A. Single-Layered Antenna

For the single-layered structure, as shown in Fig. 2, the solution at the $z = z_1$ plane due to current at $z = z_1^-$ is given

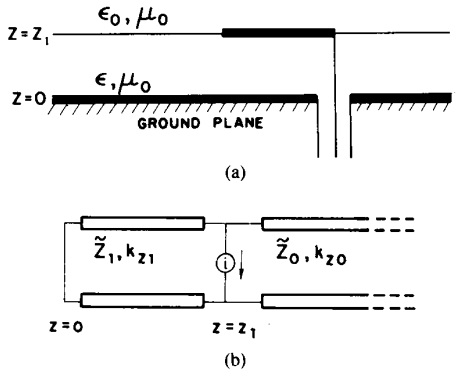

Fig. 2. Single-layered microstrip antenna. (a) Physical configuration. (b) Transmission line model.

by

$$\tilde{V}_i(z_1,z_1)=\frac{1}{\overleftarrow{\tilde{Y}}(z_1)+\overrightarrow{\tilde{Y}}(z_1)} \tag{20}$$

where

$$\overleftarrow{\tilde{Y}}(z_1)=-j\tilde{Y}_1\cot(k_{z1}z_1)\qquad \overrightarrow{\tilde{Y}}(z_1)=\overrightarrow{\tilde{Y}}_0 \tag{21}$$

are the leftward- and rightward-looking modal admittances, with $\tilde{Y}_{0,1}$ and $k_{z0,1}$ representing the characteristics modal admittances and wavenumbers in free space and in the dielectric layer, respectively, as defined by (7), (8), and Fig. 2(b). The Cartesian Green's dyad $\underline{\tilde{\mathbf{G}}}_{1,1}^{e}$ needed in (14) is given now by substituting (20) into (16), using (17) for the Cartesian projections. The incident field $\tilde{\mathbf{E}}_1^{\text{inc}}$ needed in (14) is obtained using (19). Assuming that the probe is located at $z' = z_1^-$, we have

$$\tilde{V}_v(z_1,z_1)=\frac{-\overrightarrow{\tilde{Z}}(z_1)}{\overleftarrow{\tilde{Z}}(z_1)+\overrightarrow{\tilde{Z}}(z_1)} \tag{22}$$

wherein $\overleftrightarrow{\tilde{Z}}$ are determined from (21).

B. Double-Layered Antenna

For the double-layered structure shown in Fig. 3, one needs to calculate four two-by-two dyads $\underline{\tilde{\mathbf{G}}}_{n,j}^{e}$, with $n = 1, 2$ and $j = 1, 2$. These dyads are expressed via (16) in terms of the modal voltages $\tilde{V}_i'(z_n, z_j)$ and $\tilde{V}_i''(z_n, z_j)$. Since these functions are continuous over the source plane $z' = z_j$, we may evaluate them with the source located either at $z' = z_j^-$ or at $z' = z_j^+$. For convenience, we have chosen to place the sources at z_1^+ and z_2^-, obtaining from the transmission line equation (Fig. 3(b)) for either the TM or TE modes

$$\tilde{V}_i(z_j,z_j)=\frac{-1}{\overleftarrow{\tilde{Y}}(z_j)+\overrightarrow{\tilde{Y}}(z_j)},\qquad j=1,2$$

$$\tilde{V}_i(z_2,z_1)=-\frac{\tilde{Z}_2}{2}\,\frac{\overrightarrow{\tilde{Y}}(z_1)+\tilde{Y}_2}{\overleftarrow{\tilde{Y}}(z_1)+\overrightarrow{\tilde{Y}}(z_1)}\,[e^{-jk_{z2}t_2}+\overrightarrow{\tilde{\Gamma}}(z_1^+)e^{jk_{z2}t_2}]$$

$$\tilde{V}_i(z_1,z_2)=-\frac{\tilde{Z}_2}{2}\,\frac{\overleftarrow{\tilde{Y}}(z_2)+\tilde{Y}_2}{\overleftarrow{\tilde{Y}}(z_2)+\overrightarrow{\tilde{Y}}(z_2)}\,[e^{-jk_{z2}t_2}+\overleftarrow{\tilde{\Gamma}}(z_2^-)e^{jk_{z2}t_2}]. \tag{23}$$

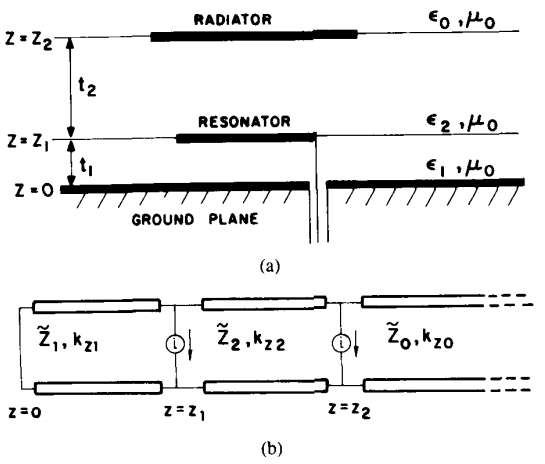

Fig. 3. Double-layered microstrip antenna. (a) Physical configuration. (b) Transmission line model.

Here, $t_{1,2}$ are the widths of the first and second layers, respectively, $\tilde{Y}_{0,1,2}$ and $k_{z0,1,2}$ are the modal admittances and wavenumbers in free space and in the first and second layers, respectively (see Fig. 3),

$$\overleftarrow{\tilde{Y}}(z_1) = -j\tilde{Y}_1 \cot(k_{z1}t_1) \qquad \overrightarrow{\tilde{Y}}(z_1) = \tilde{Y}_2 \frac{1-\overrightarrow{\tilde{\Gamma}}(z_1^+)}{1+\overrightarrow{\tilde{\Gamma}}(z_1^+)}$$

$$\overleftarrow{\tilde{Y}}(z_2) = \tilde{Y}_2 \frac{1-\overleftarrow{\tilde{\Gamma}}(z_2^-)}{1+\overleftarrow{\tilde{\Gamma}}(z_2^-)} \qquad \overrightarrow{\tilde{Y}}(z_2) = \tilde{Y}_0 \tag{24}$$

are the leftward- or rightward-looking modal admittances at $z_{1,2}$, and

$$\overrightarrow{\tilde{\Gamma}}(z_1^+) = \frac{\tilde{Z}_0 - \tilde{Z}_2}{\tilde{Z}_0 + \tilde{Z}_2} e^{-2jk_{z2}t_2}$$

$$\overleftarrow{\tilde{\Gamma}}(z_2^-) = \frac{j\tilde{Z}_1 \tan(k_{z1}t_1) - \tilde{Z}_2}{j\tilde{Z}_1 \tan(k_{z1}t_1) + \tilde{Z}_2} e^{-2jk_{z2}t_2} \tag{25}$$

are the rightward- and leftward-looking reflection coefficients at z_1^+ and z_2^-, respectively. The incident fields $\tilde{\mathbf{E}}_{1,2}^{\text{inc}}$ in (14) are found from (19) with $V_v(z_1, z_1)$ given by (22) and

$$\tilde{V}_v(z_2, z_1) = -\frac{1}{2} \frac{\overrightarrow{\tilde{Z}}(z_1) + \tilde{Z}_2}{\overleftarrow{\tilde{Z}}(z_1) + \overrightarrow{\tilde{Z}}(z_1)} [e^{-jk_{z2}t_2} + \overrightarrow{\tilde{\Gamma}}(z_1^+) e^{jk_{z2}t_2}]. \tag{26}$$

IV. Application of the Conjugate Gradient Algorithm

The basic CG scheme proposed by Van Den Berg [20], which is similar to [22, case A], is cast in the spectral domain so as to solve (14). For the two-layer case, the algorithm is listed in the Appendix. As seen in steps 5–8 of the algorithm, the work areas denoted $\mathbf{W}_{1,2}$ are used both for the current and field correction functions. However, no current information is retained in order to achieve substantial storage savings. Further explanations on the specific operations, using the same basic notations, are included in [23] and are not repeated here.

Once the iterative process has been terminated with a specified $\text{err}^{(n)}$, the scattered field is at hand either in its spatial or spectral form. In principle, the spectral form could be used to present the radiated pattern. However, the sampling interval in the spectral domain may be too wide and interpolation is then needed to provide convenient angular resolution in the visible range. Practically, this is done by first computing the equivalent current distribution at $z = z_2$ (or the actual current distribution at $z = z_1$ for the single layer case) using the following relationship:

$$\mathbf{J}^{eq} = F^{-1}\{(\underline{\tilde{\mathbf{G}}}_{2,2}^{e})^{-1} \cdot \tilde{\mathbf{E}}_2\}. \tag{27}$$

This equivalent current contains the actual $\mathbf{J}_2$ plus a transformation of $\mathbf{J}_1$ to $z = z_2$, hence it is not necessarily of finite support. The samples of this distribution are now integrated directly like an array to provide the pattern at any chosen angular interval. In addition to this, *actual* $\mathbf{J}_1$ and $\mathbf{J}_2$ distributions may be computed from $\mathbf{E}_1$ and $\mathbf{E}_2$ by inverting the entire four-by-four $\underline{\tilde{\mathbf{G}}}$ matrix of (14).

V. Results

A. Single Patch Antenna

The single patch microstrip antenna shown in Fig. 2 was spatially sampled by five-by-five and a six-by-six grid. There were a total of N_x by N_y sampling points in the two-dimensional discrete Fourier transform. Patch dimensions are $(\lambda/(2\sqrt{\epsilon_r}))^2$, with $\epsilon_r = 2.45$, which make the sampling interval, denoted below as Δ, a reasonable 0.076 λ or smaller. The width of the dielectric layer was $\lambda/100$. The feeding point was placed at three locations as follows:

1) feed connected by a 1 λ microstrip segment to the center of the antenna edge,
2) feed connected by a $\lambda/3$ microstrip segment to the center of the antenna edge,
3) feed connected directly to the center of the antenna edge.

It turns out that abrupt changes in geometry, such as the narrow microstrip lines, have an adverse effect on convergence rates. The longer the line, the worse convergence will be, as shown in Table I. Other fine additions or changes in geometry show similar effects, as do variations in size, shape, and sampling interval. These changes in convergence behavior are not due to the higher spectral content of the finer structures, because utilization of the FFT defines a fixed unit cell in the spectral domain as well as in the spatial one. This unit cell is linked to a spatial low-pass filtering which is exploited by the finite spatial sampling rate. It is rather the nature of the operator, including geometry and samplings, that influences convergence. Representative convergence rates are summarized in Table I.

Relative rms error convergence curves are shown in Fig. 4 for the cases of 1 λ line and for direct feeding (cases 1 and 3, respectively). From Table I and looking at this figure, it becomes apparent that the addition of the feeding line greatly inhibits convergence as compared to the direct feeding case. The longer the line is, the slower convergence becomes. This problematic behavior is probably true for many finer struc-

TABLE I
CONVERGENCE RATES FOR THE SINGLE-LAYER CASE

Case	N_x	N_y	Δ/λ	Number of Sampling Points on Patch	Number of Iteration	Final RMS Error (Percent)
1	36	20	0.032	6 × 6	57	10
2	36	20	0.032	6 × 6	50	4
3	30	16	0.076	5 × 5	21	0.9

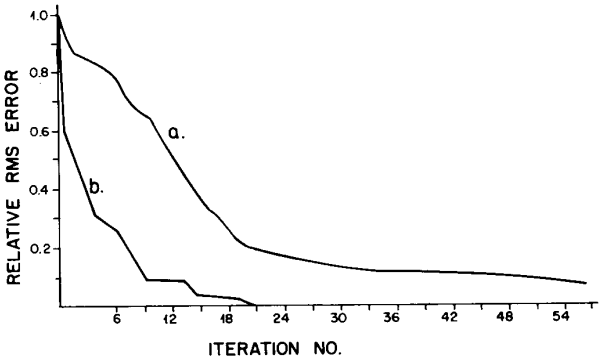

Fig. 4. Convergence curve for single-layered microstrip antenna. (a) Fed by long transmission line. (b) Fed by pin.

tures. Another example may be found in [22], where the problem of a thin wire uses up the theoretical maximum number of iterations, i.e., the number of degrees of freedom of the problem (16 in that case).

Radiation patterns for both principal planes are shown in Figs. 5(a) and 5(b), for case 3. Comparison with measured patterns is very good within the main beam. Computed and measured 3-dB beamwidths are 104.4° and 87° at the H- and E-planes, respectively. Cross polarization at the E-plane, shown in Fig. 5(b), is of the order of -23 dB, in agreement with on-axis measurements. Small discrepancies between calculations and measurements appear, however, beyond $\pm 55°$ relative to broadside, manifesting spill over the actual finite ground plane, which may be contrasted with the idealized infinite ground plane model used for the finite-sized antenna. The current distribution on the patch surface for case 3 is shown in Fig. 6. Deviation from the commonly assumed cosine-type distribution in the E-plane is clearly visible.

B. Double-Patch Antenna.

For this case, the smaller (closer to ground plane) patch is $(\lambda/(2\sqrt{\epsilon_{r1}}))^2$ large, with $\epsilon_{r1} = 2.45$ being the dielectric constant in the first layer, and is sampled by five-by-five samples. The upper patch is either larger than the lower one, or of the same size, being represented by seven-by-seven or five-by-five samples, respectively, with the same sampling rate. The dielectric constant of the second layer was $\epsilon_{r2} = 2.2$ and the width of the layers were $t_1 = t_2 = \lambda/100$. Again, geometry has a profound effect on convergence rates. The sizes of the patch elements, the separation between them, and sampling interval make a difference. Table II summarizes some of the findings for pin-fed resonator patches. Cases 1 and 2 differ in the size of the upper (radiating) element. It is readily seen that the smaller element case 1 converges faster than case 2 of the larger one. In addition, even when the two patches are of the same size (cases 2 and 3), but the frequency is lower so that Δ/λ is smaller (case 3), convergence again tends to be slower, probably because of the finer nature of this problem. A representative convergence curve for case 1 of Table II is shown in Fig. 7. Radiation patterns for the H-and E-planes of this case are confronted with experiments in Fig. 8(a) and (b), respectively. The 3-dB beamwidths are 77° and 79°, at the H and E cuts, respectively, computationally as well as experimentally. The broadside cross-polarized component at the E-plane is lower than the single patch case, about -30 dB, though it increases towards -18 dB at the edges. This result, too, has been observed experimentally. As in the single patch case, discrepancies may occur beyond $\pm 55°$ away from broadside, for similar reasons. The equivalent current on the radiating patch plane is computed in the manner described in Section IV (see (27)). The result is shown in Fig. 9. This distribution is somewhat smoother than the single-patch case (Fig. 6), and furthermore, being an equivalent current distribution, it decays gradually away from the patch on the upper plane. For this reason, the double-layered antenna has a more efficient aperture than the single-layered one.

VI. Conclusion

The advantages and limitations of the CG algorithm hold for the microstrip antenna application as they do for other cases. The convergence rate is again found sensitive to the geometry, as mentioned already in [23]. The more rapidly varying the geometry is, the slower convergence will be. This fact, while not precluding the use of the CG algorithm, makes the

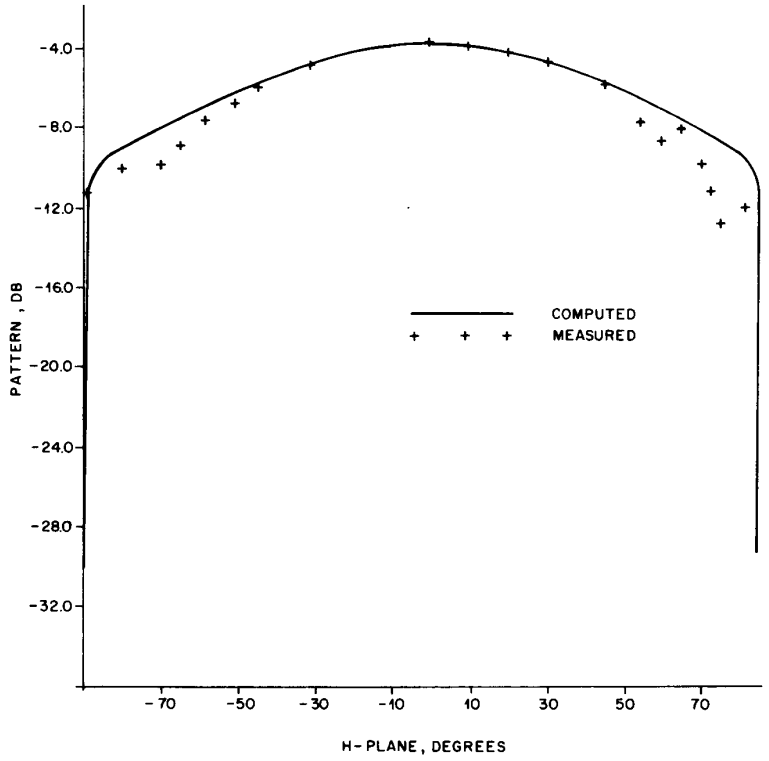

(a)

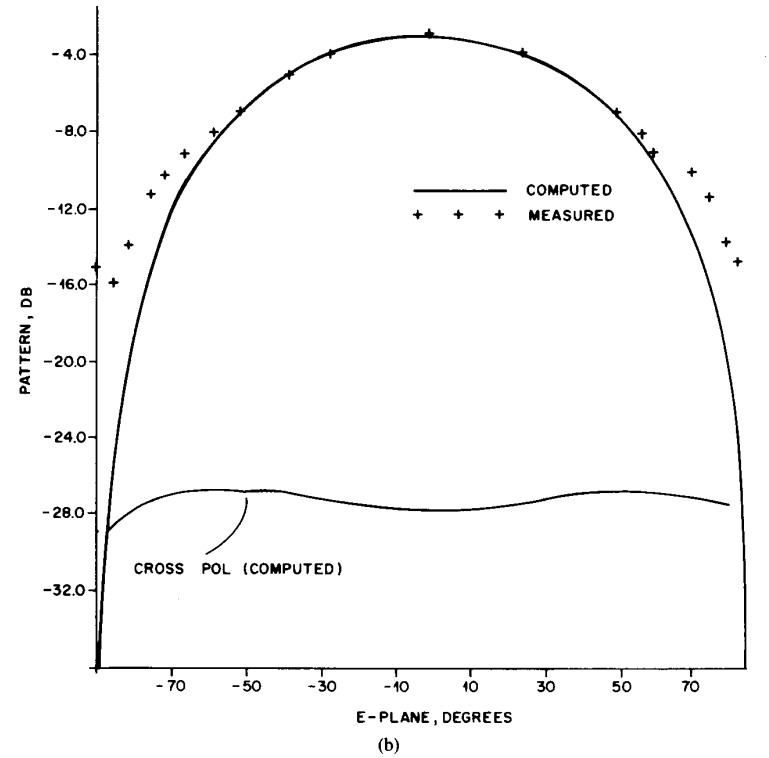

(b)

Fig. 5. Radiation pattern of single-layered antenna fed by pin. (a) *H*-plane. (b) *E*-plane.

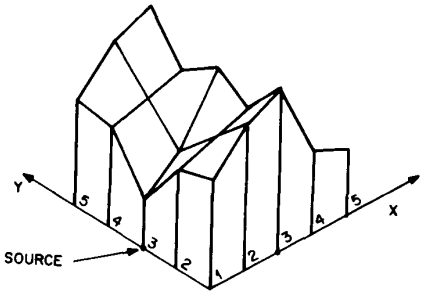

Fig. 6. Co-polarized current distribution on single-layered microstrip antenna fed by pin.

TABLE II
CONVERGENCE RATES FOR THE DOUBLE LAYER CASE

Case	N_x	N_y	Δ/λ	Number of Sampling Points on Resonator	Number of Sampling Points on Radiator	Number of Iterations	Final RMS Error (Percent)
1	30	16	0.076	5 × 5	5 × 5	28	4.5
2	30	16	0.076	5 × 5	7 × 7	83	3
3	30	16	0.053	5 × 5	7 × 7	80	7

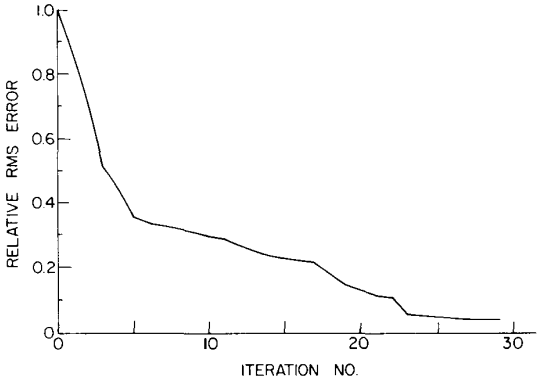

Fig. 7. Convergence curve for double-layered microstrip antenna fed by pin.

computational cost unpredictable when a realistic, finite error criterion is used. For the problems treated here, conventional moment methods may supply equivalent results since the overall number of unknowns is not very large. The potential for larger problems has been discussed in [23]; however, few large problems have been reported in the literature so far, apart from theoretical considerations. For our small problem, full vector current distributions have been obtained, as have radiated fields, including co-polarized as well as cross-polarized components. The fact that the structure must be described by a rectangular sampling grid has a bearing upon feed modeling like the elementary probe used above. This probe, being restricted to a specific sampling point at present, deserves a closer look in the future. This may be important for accurate reactance calculations.

APPENDIX

THE SPECTRAL CONJUGATE GRADIENT ALGORITHM FOR THE DOUBLE-LAYERED CASE

1) Set the initial guess $\tilde{\mathbf{E}}_j^{(0)}$ for the scattered field at both planes z_j, $j = 1, 2$.

At step n, go to 2).

2) $$\mathrm{err}^{(n)} = \sum_{j=1}^{2} \sum_{D_j} |\mathbf{E}_j^{(n)} + \mathbf{E}_j^{\mathrm{inc}}|^2.$$

3) $$\mathbf{W}_j^{(n)} = \theta_j \left[F^{-1} \sum_{i=1}^{2} \tilde{\mathbf{G}}_{j,i}^{e} \cdot F\{\theta_i \mathbf{E}_i^{(n)*}\} \right]^*, \qquad j = 1, 2.$$

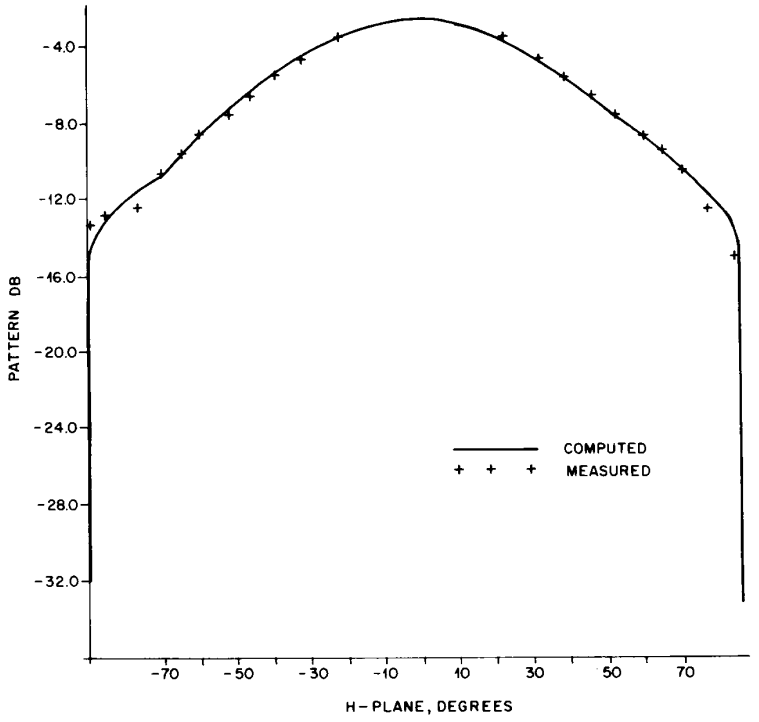

(a)

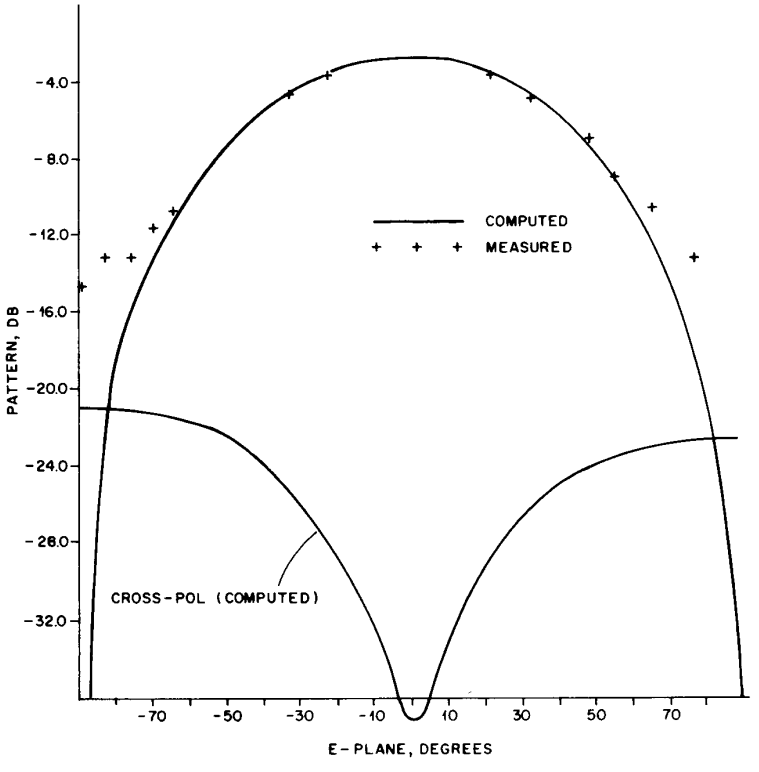

(b)

Fig. 8. Radiation pattern of double-layered antenna fed by pin. (a) *H*-plane. (b) *E*-plane.

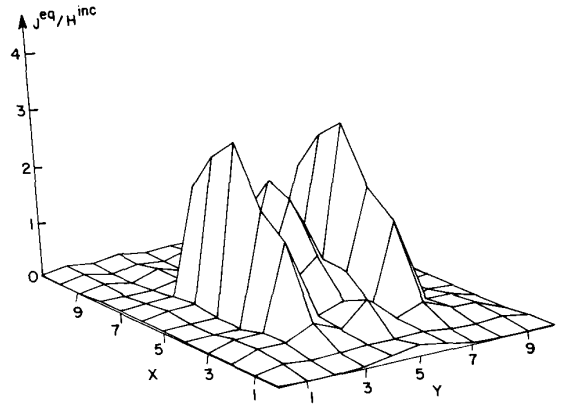

Fig. 9. Co-polarized equivalent current distribution on upper face of double-layered microstrip antenna. Patch is located between $3 \le x \le 7$ and $3 \le y \le 7$, source is at (3, 5).

4) $a^{(n)} = \sum_{j=1}^{2} \sum_{D_j} |\mathbf{W}_j^{(n)}|^2.$

5) $\mathbf{W}_j^{(n)} = \mathbf{W}_j^{(n)} + \dfrac{a^{(n)}}{a^{(n-1)}} \mathbf{W}_j^{(n-1)},$

$j = 1, 2$ (current terms).

6) $\mathbf{W}_j^{(n)} = F^{-1} \sum_{i=1}^{2} \underline{\tilde{G}}_{j,i} \cdot F\{\mathbf{W}_i^{(n)}\},$

$j = 1, 2$ (field terms).

7) $b^{(n)} = \sum_{j=1}^{2} \sum_{D_j} |\mathbf{W}_j^{(n)}|^2, \qquad \eta^{(n)} = \dfrac{a^{(n)}}{b^{(n)}}.$

8) $\mathbf{E}_j^{(n)} = \mathbf{E}_j^{(n)} - \eta^{(n)} \mathbf{W}_j^{(n)}, \qquad j = 1, 2$

9) Go to step 2.

References

[1] A. Sabban, "A new broadband stacked two layer microstrip antenna," in *1983 Int. IEEE/AP-S Symp. Digest,* Houston, TX, pp. 63-66.

[2] A. G. Derneryd, "Linearly polarized microstrip antennas," *IEEE Trans. Antennas Propagat.,* vol. AP-24, pp. 846-851, Nov. 1976.

[3] R. E. Munson, "Corner fed microstrip antennas and microstrip phased arrays," *IEEE Trans. Antennas Propagat.,* vol. AP-22, pp. 74-78, Jan. 1974.

[4] A. G. Derneryd, "A theoretical investigation of the rectangular microstrip antenna element," *IEEE Trans. Antennas Propagat.,* vol. AP-26, pp. 532-533, July 1978.

[5] J. Q. Howell, "Microstrip antennas," *IEEE Trans. Antennas Propagat.,* vol. AP-23, pp. 90-93, Jan. 1975.

[6] C. W. Carwin, R. E. Munson, L. T. Ostwald, and K. G. Schroeder, "Missile based mounted microstrip antennas," *IEEE Trans. Antennas Propagat.,* vol. AP-25, pp. 604-610, Sept. 1977.

[7] L. C. Shen, S. A. Long, M. R. Allerding, and M. D. Walton, "Resonant frequency of a circular disk, printed circuit antenna," *IEEE Trans. Antennas Propagat.,* vol. AP-25, pp. 595-596, July 1977.

[8] Y. T. Lo, D. Solomon, and W. F. Richards, "Theory and experiment on microstrip antenna," *IEEE Trans. Antennas Propagat.,* vol. AP-27, pp. 137-145, Mar. 1979.

[9] W. F. Richards, Y. T. Lo, and D. D. Harrison, "An improved theory for microstrip antennas and applications," *IEEE Trans. Antennas Propagat.,* vol. AP-27, pp. 38-46, Jan. 1979.

[10] A. C. Derneryd, "Design of microstrip patch antenna elements," Rome Air Development Center, Griffiss AFB, NY, Tech. Rep. RADC-TR-78-46, Feb. 1978.

[11] A. G. Derneryd and A. G. Lind, "Extended analysis of rectangular microstrip resonator antennas," *IEEE Trans. Antennas Propagat.,* vol. AP-27, pp. 846-849, Nov. 1979.

[12] P. K. Agrawal and M. C. Bailey, "An analysis for microstrip antennas," *IEEE Trans. Antennas Propagat.,* vol. AP-25, pp. 756-759, Nov. 1977.

[13] E. H. Newman and P. Tulyathan, "Analysis of microstrip antennas using moment methods," *IEEE Trans. Antennas Propagat.,* vol. AP-29, pp. 47-53, Jan. 1981.

[14] D. M. Pozar and D. H. Schaubert, "Analysis of an infinite array of rectangular microstrip patches with idealized probe feeds," *IEEE Trans. Antennas Propagat.,* vol. AP-32, pp. 1101-1107, Oct. 1984.

[15] D. M. Pozar, "General relations for a phased array of printed antennas derived from infinite current sheets," *IEEE Trans. Antennas Propagat.,* vol. AP-33, pp. 498-504, May 1985.

[16] D. C. Chang, "Analytical theory of unloaded rectangular microstrip patch," *IEEE Trans. Antennas Propagat.,* vol. AP-29, pp. 54-62, Jan. 1981.

[17] T. Itoh and W. Menzel, "A full wave analysis method for open microstrip structures," *IEEE Trans. Antennas Propagat.,* vol. AP-29, pp. 63-68, Jan. 1981.

[18] P. B. Katehi and N. G. Alexopoulos, "On the modeling of electromagnetically coupled microstrip antenna—The printed strip dipole," *IEEE Trans. Antennas Propagat.,* vol. AP-32, pp. 1179-1186, Nov. 1984.

[19] C. H. Chen, A. Tulintseff, and R. M. Sorbello, "Broadband two-layered microstrip antenna," in *1984 Int. IEEE/AP-S Symp. Digest,* Boston, MA, 1984, pp. 251-254.

[20] P. M. van den Berg, "Iterative computational techniques in Scattering based upon the integrated square error criterion," *IEEE Trans. Antennas Propagat.,* vol. AP-32, pp. 1063-1071, Oct. 1984.

[21] M. R. Hestenes and E. Steifel, "Method of conjugate gradients for solving linear systems," *J. Res. Nat. Bur. Stand.,* vol. 49, pp. 409-436, 1952.

[22] T. K. Sarkar and E. Arvas, "On a class of finite step iterative methods (Conjugate Directions) for the solution of an operator equation arising in electromagnetics," *IEEE Trans. Antennas Propagat.,* vol. AP-33, pp. 1058-1066, Oct. 1985.

[23] R. Kastner and R. Mittra, "Iterative analysis of finite-sized planar frequency selective surfaces with rectangular patches or perforations," *IEEE Trans. Antennas Propagat.,* vol. AP-35, pp. 372-377, Apr. 1987.

[24] L. B. Felsen and N. Marcuvitz, *Radiation and Scattering of Waves.* Englewood Cliffs, NJ: Prentice-Hall, 1973, ch. 2, pp. 185-217.

Raphael Kastner (S'80-M'82-SM'87) received the B.S. (summa cum laude) and M.S. degrees from the Technion, Israel Institute of Technology, Haifa, and the Ph.D. degree from the University of Illinois, Urbana, in 1973, 1976, and 1982, respectively.

From 1976 to 1979 he was employed by RAFAEL, Haifa, Israel, where he conducted research on scanning arrays and numerical techniques. He joined the University of Illinois in 1979 first as Research Assistant and later as a Visiting Research Associate, where he worked on scattering analysis in the spectral domain. From 1982 to 1986 he headed the Antenna Research Group at RAFAEL. He was a Visiting Assistant Professor at Syracuse University and a Visiting Scholar at the University of Illinois during 1987, prior to his return to RAFAEL.

Dr. Kastner is a member of Tau Beta Pi and Eta Kappa Nu.

Ehud Heyman (S'80-M'82-SM'88), for a photograph and biography please see page 437 of the May 1983 issue of this TRANSACTIONS.

Albert Sabban was born in Alexandria, Egypt, in 1951. He received the B.Sc. and M.Sc. degrees in electrical engineering from Tel-Aviv University, Tel Aviv, Israel, in 1976 and 1986, respectively. He is currently working toward the Ph.D. degree at the University of Colorado, Boulder.

In 1976 he joined the armament development authority, RAFAEL, where he serves as a Senior Antenna and Microwave Engineer and Project Supervisor. From 1984 to 1987 he was a leader of an Antenna Group in RAFAEL. He is now on a sabbatical leave from RAFAEL and has been employed as a Graduate Research Assistant at the University of Colorado.